MOLECULAR AND CELLULAR BIOLOGY, May 2011, p. 1983–1996 Vol. 31, No. 10
0270-7306/11/$12.00 doi:10.1128/MCB.00609-10

FERM Domain Phosphoinositide Binding Targets Merlin to the Membrane and Is Essential for Its Growth-Suppressive Function[▽]

Timmy Mani,[1] Robert F. Hennigan,[1]† Lauren A. Foster,[1] Deborah G. Conrady,[2] Andrew B. Herr,[2] and Wallace Ip[1]*

Departments of Cancer and Cell Biology[1] and Molecular Genetics, Biochemistry, and Microbiology,[2] University of Cincinnati, Cincinnati, Ohio 45267

Received 26 May 2010/Returned for modification 4 July 2010/Accepted 22 February 2011

The neurofibromatosis type 2 tumor suppressor protein, merlin, is related to the ERM (ezrin, radixin, and moesin) family of plasma membrane-actin cytoskeleton linkers. For ezrin, phosphatidylinositol 4,5-bisphosphate (PIP_2) binding to the amino-terminal FERM domain is required for its conformational activation, proper subcellular localization, and function, but less is known about the role of phosphoinositide binding for merlin. Current evidence indicates that association with the membrane is important for merlin to function as a growth regulator; however, the mechanisms by which merlin localizes to the membrane are less clear. Here, we report that merlin binds phosphoinositides, including PIP_2, via a conserved binding motif in its FERM domain. Abolition of FERM domain-mediated phosphoinositide binding of merlin displaces merlin from the membrane and releases it into the cytosol without altering the folding of merlin. Importantly, a merlin protein whose FERM domain cannot bind phosphoinositide is defective in growth suppression. Retargeting the mutant merlin into the membrane using a dual-acylated amino-terminal decapeptide from Fyn is sufficient to restore the growth-suppressive properties to the mutant merlin. Thus, FERM domain-mediated phosphoinositide binding and membrane association are critical for the growth-regulatory function of merlin.

Merlin, the neurofibromatosis type 2 (NF2) tumor suppressor protein, is a member of the band 4.1/ERM family of plasma membrane-actin cytoskeleton linkers (6). Like other members of this family, merlin has a globular amino-terminal FERM (four point one, ezrin, radixin, and moesin) domain followed by an α-helical coiled-coil domain and a carboxy-terminal domain (28, 58). The amino and carboxy termini of merlin and ERM proteins can bind one another; thus, these proteins can exist in two states, open and closed (6, 57). Interconversion between the two states is regulated by phosphorylation near the carboxy terminus. For ERM, the best-studied phosphorylated residue is a conserved threonine (ezrin T567, radixin T564, and moesin T558) (42). Likewise, for merlin, the phosphorylated residue is S518 (56); only the dephosphorylated, closed conformation is believed to be growth suppressive (44, 55, 57).

For ezrin, phosphorylation and the ability to undergo conformational changes are regulated by the binding of the FERM domain to the membrane lipid, phosphoinositide-(4,5)-bisphosphate (PIP_2) (3, 14). PIP_2 facilitates the binding of ERM proteins to membrane proteins (21, 24). Recent studies showed that even after ezrin is phosphorylated, PIP_2 binding is the primary regulator of ERM membrane association (19).

The residues implicated in PIP_2 binding are conserved among the ERM proteins (17, 36, 58), and sequence homology suggests that there are potential PIP_2 binding motifs in the merlin FERM domain. Exogenous addition of PIP_2 enhances the binding of a regulatory cofactor for Na^+-H^+ exchange (NHE-RF) to merlin *in vitro* (16), suggesting that PIP_2 binding might play an important role in merlin function. Notably, three of the six (K79, K269, and E270) merlin residues in the predicted PIP_2 binding motif are sites of mutations in NF2 patients (58).

Recent evidence suggests that association with the plasma membrane is important for merlin function (10, 11, 31–33, 41, 43). A significant fraction of total cellular merlin associates with cholesterol- and glycosphingolipid-rich plasma membrane domains in which numerous signaling events occur (8, 11, 61). Precisely how merlin is linked to the membrane remains unknown; however, PIP_2 binding is a likely candidate mechanism (39, 51). We therefore hypothesized that phosphoinositide binding regulates the localization and growth-suppressive function of merlin. We report that merlin binds phosphorylated phosphoinositides (PIP) and that PIP binding via a conserved binding motif in the FERM domain is necessary for its proper subcellular localization, its association with membrane domains, and intracellular dynamics. Mutating the FERM domain PIP binding sites does not affect the overall folding or the phosphorylation status of merlin at S518. Importantly, FERM domain PIP binding regulates the ability of merlin to inhibit cyclin D1 expression, cell proliferation, and colony formation. Furthermore, retargeting the mutant merlin into membrane domains using a dual-acylated amino-terminal decapeptide from Fyn is sufficient to restore the growth-suppressive function to the mutant merlin. Collectively, our data indicate that FERM domain-mediated phosphoinositide binding and membrane association are critical for the growth-regulatory function of merlin.

* Corresponding author. Mailing address: Department of Cancer and Cell Biology, Vontz Center for Molecular Studies, 3125 Eden Avenue, University of Cincinnati, Cincinnati, OH 45267-0521. Phone: (513) 558-3614. Fax: (513) 558-4454. E-mail: wallace.ip@uc.edu.

† Present address: Division of Experimental Hematology and Cancer Biology, Cincinnati Children's Hospital Medical Center, Cincinnati OH 45229.

▽ Published ahead of print on 14 March 2011.

MATERIALS AND METHODS

Reagents and supplies. All reagents were from Sigma (St. Louis, MO) unless otherwise noted. PIP strips, PIP arrays, and glutathione S-transferase–phospholipase C-δ (GST-PLC-δ) were from Echelon Biosciences, Inc. (Salt Lake City, UT). *N*-Octyl-β-D-glucopyranoside (NOG) was from Amresco Inc. (Solon, OH).

Cell culture. NIH 3T3 cells (ATCC, Manassas, VA) were maintained in Dulbecco's modified Eagle's medium (DMEM; Cellgro, Manassas, VA) containing 10% fetal calf serum (FCS; ATCC) and 100 units/ml penicillin-streptomycin (Invitrogen, Carlsbad, CA). SC4 cells, an immortalized, transformed Schwann cell line derived from the $Nf2^{\Delta 2/\Delta 2}$ (*Nf2* with an in-frame deletion of exon 2) mouse (15, 45), were maintained in DMEM containing 10% fetal bovine serum (FBS; Serum Source International, Charlotte, NC) and 100 units/ml penicillin-streptomycin. Cells were transiently transfected using Lipofectamine 2000 (Invitrogen).

DNA cloning. Human merlin isoform 1 (NM_000268) fused to a FLAG tag at the amino terminus and the T7-tagged merlin FERM domain (amino acids [aa] 1 to 295) were cloned into pcDNA3 (Invitrogen) (61). QuikChange site-directed mutagenesis (Stratagene, La Jolla, CA) was used to introduce mutations. The following primers (IDT, Coralville, IA) were used (changes to asparagine [N] are italicized): for the K79N and K80N (2N merlin) mutations, 5′-GCC TGG CTC AAA ATG GAC *AAT AAT* GTA CTG GAT CAT GAT G-3′ (forward); for the K269N and E270N mutations, 5′-CGA AAC ATC TCG TAC AGT GAC *AAT AAT* TTT ACT ATT AAA CCA CTG-3′ (forward); for the K278N and K279N mutations, 5′-CCA CTG GAT *AAC AAC* ATT GAT GTC TTC AAG-3′ (forward). For GST-merlin FERM fusion expression, wild-type (WT) and mutant 6N merlin (merlin with the mutations K79N, K80N, K269N, E270N, K278N, and K279N) FERM domains were cloned into pGEX4T2 (GE Health Care, Piscataway, NJ). Full-length WT merlin, full-length merlin 6N, or green fluorescent protein (GFP; control) was cloned into the pCDH-CMV-MCS-EF1-puromycin lentivirus vector (System Biosciences, Mountain View, CA). To generate the Fyn-tagged construct, nucleotides encoding the first 10 amino acids of Fyn ($Fyn_{1\text{-}10}$; MGCVQCKDKE) were first cloned into the pCDH-CMV-MCS-EF1-puromycin vector. Full-length merlin 6N was then cloned into the Fyn tag-containing vector to obtain the Fyn-merlin 6N construct. All constructs were verified by DNA sequencing and Western blotting.

Full-length WT merlin, full-length merlin 6N, or GFP (control) cloned into the pCDH-CMV-MCS-EF1-puromycin lentivirus vector was used to produce lentiviral particles at the Viral Vector Core, Translational Core Laboratories, Cincinnati Children's Medical Center. All biosafety precautions were followed during virus handling as per the University of Cincinnati's biosafety level 2 criteria.

Protein purification. Rosetta 2(DE3) competent cells (Novagen, Madison, WI) transformed with plasmids encoding fusion proteins were plated onto LB plates containing either ampicillin (100 mg/liter) and chloramphenicol (30 mg/liter) for GST fusion proteins or kanamycin (30 mg/liter) for His fusion proteins. Colonies were grown in LB medium containing appropriate antibiotics at 37°C until the optical density at 600 nm (OD_{600}) reached 1.8. Pelleted cells were resuspended in fresh cooled (8°C) medium and induced with 0.1 mM isopropyl-β-D-thiogalactopyranoside (IPTG; Amresco) at 20°C overnight. Following centrifugation, induced cells were lysed, sonicated, and spun to recover the soluble proteins in the supernatant. The supernatant was then incubated with glutathione-Sepharose 4B (GE Health Care) for GST-tagged proteins or with Ni-Sepharose 6 Fast Flow (GE Health Care) for His-tagged proteins. Proteins bound to beads were eluted, dialyzed, and stored as aliquots at −80°C after determination of protein concentration. His_6-Cerulean-merlin-Venus-Strep tag proteins (full-length WT and 6N) (Venus is a GFP mutant with a yellow-shifted emission spectrum, and Cerulean is a GFP mutant with blue-shifted emission spectrum) were purified using a dual-affinity tag protocol as previously described (22).

Protein-lipid overlay assay. PIP strips and PIP arrays were blocked for 1 h in phosphate-buffered saline (PBS) containing 0.1% Tween 20 (PBST) and 3% fatty acid-free bovine serum albumin (BSA). They were then incubated with 1 μg/ml of the protein indicated on the figures in blocking solution for 1 h and washed with PBST, and the bound proteins were analyzed by immunoblot analysis.

Intrinsic tryptophan fluorescence. GST-FERM WT or 6N protein intrinsic fluorescence measurements were carried out using a Horiba Jobin Yvon Fluorolog-3 spectrofluorometer. Purified proteins were analyzed at a concentration of 1 μM in 10 mM Tris (pH 7.5)–150 mM NaCl at room temperature. Samples were excited at 295 nm with a 5-nm slit width, and fluorescence emission spectra were recorded from 300 nm to 500 nm at 1-nm intervals with a 5-nm slit width.

Chymotryptic digestion. Limited in-gel digestion of GST-FERM WT or 6N purified proteins using different concentrations of chymotrypsin was carried out as described previously (9).

FRET spectrofluorometry. His_6-Cerulean, His_6-Cerulean-6-Venus-Strep (with Cerulean and Venus fused in frame and separated by a 6-residue linker), and full-length wild-type and mutant 6N merlin proteins (His_6-Cerulean-merlin-Venus-Strep) were purified and used for fluorescent resonance energy transfer (FRET) measurements as previously described (22).

CD. Far-UV circular dichroism (CD) spectra of full-length wild-type and mutant 6N merlin proteins (His_6-Cerulean-merlin-Venus-Strep) were acquired in an Aviv 215 circular dichroism spectrometer. The standard extinction coefficient at A_{280} is 59,375 M^{-1} cm^{-1}. CD spectra were taken from 260 to 180 nm after dialysis into buffer containing 20 mM sodium phosphate, pH 7.4, 150 mM NaF, and 1 mM β-mercaptoethanol. Data were converted to units of mean residue ellipticity using the following formula: $[\theta] = \theta/(10 \cdot C \cdot l \cdot n_r)$, where θ is the measured ellipticity in millidegrees, C is the concentration in molar units, l is the path length in cm, and n_r is the number of residues. Secondary structure deconvolution was carried out in the CDSSTR (27) module of Dichroweb (65), and solutions from reference sets 3 and 6 were compared since these cover the full wavelength range of usable experimental data.

Analytical ultracentrifugation (AUC). Sedimentation velocity experiments of full-length wild-type and mutant 6N merlin proteins (His_6-Cerulean-merlin-Venus-Strep) were carried out using a Beckman XL-I analytical ultracentrifuge with absorbance optics. All data were collected at 36,000 rpm and 20°C in a four-hole rotor. Data were analyzed using a continuous $c(s)$ distribution model in Sedfit (54). Molecular weight estimates are based on a continuous $c(M)$ analysis in Sedfit. Samples were analyzed in 20 mM Tris, 150 mM NaCl, and 1 mM β-mercaptoethanol at 230 nm, a wavelength with minimal buffer absorbance.

GST–NHE-RF pulldown. Lysates from SC4 cells transfected with the constructs indicated on the figures were incubated with GST or GST–NHE-RF bound to glutathione beads for 1 h at 4°C. The beads were washed extensively, resuspended in SDS buffer, subjected to 10% SDS-PAGE, and immunoblotted.

Detergent extraction. A total of 1.5×10^6 NIH 3T3 cells plated overnight (day 1) onto 10-cm dishes were transiently transfected with indicated constructs (day 2). Medium was changed the following day (day 3) to regular medium. Confluent cells from each dish (day 4) were washed twice with cold Tris-buffered saline (TBS) and then lysed in cold 1% Triton X-100 (TX-100) in TBS (pH 7.5) buffer for 15 min on ice. A complete protease inhibitor cocktail (Roche) was added during cell lysis along with the phosphatase inhibitors 1 mM Na_3VO_4, 10 mM NaF, and 2 mM sodium pyrophosphate. Cell lysates were centrifuged at 15,000 × *g* for 20 min at 4°C to obtain a crude TX-100 pellet and TX-100 supernatant. The TX-100 pellet was washed once with buffer, recentrifuged, and then resuspended in lysis buffer with the addition of 100 mM NOG to partially solubilize the TX-100-insoluble membrane domains. Equal volumes of TX-100 supernatant and 100 mM NOG-soluble fractions were boiled for 5 min in 5× sample buffer and analyzed by SDS-PAGE.

OptiPrep density gradient centrifugation. Whole-cell lysates from confluent cells were analyzed by OptiPrep density gradient centrifugation as previously described (61).

Subcellular fractionation. Forty-eight hours posttransfection, confluent NIH 3T3 cells were subjected to fractionation as previously described (31) with the following modification. Following recovery of the cytosolic fraction (C), the membrane pellet (M) was directly extracted with modified radio immunoprecipitation assay (RIPA) buffer (50 mM Tris, pH 7.4, 150 mM NaCl, 1% TX-100, 0.1% SDS, 0.5% sodium deoxycholate, 1 mM EDTA, and protease and phosphatase inhibitors) for 30 min at 4°C.

Immunoblot analysis. Proteins transferred onto nitrocellulose membranes after SDS-PAGE were blocked overnight at 4°C in PBS containing 1% fish gelatin. The following primary antibodies were diluted in blocking buffer containing 0.1% Tween 20 and incubated with the membrane for 1 h at room temperature: anti-merlin A19 (Santa Cruz Biotechnology, Santa Cruz, CA) at 1:1,000, anti-merlin C18 (Santa Cruz) at 1:1,000, anti-pS518 merlin (Rockland, Gilbertsville, PA) at 1:1,000, anti-GST (Sigma) at 1:5,000, anti-His (Applied Biological Materials, Richmond, BC, Canada) at 1:1,000, anticaveolin (BD Biosciences, San Jose, CA) at 1:5,000, antiactin (Sigma) at 1:20,000, anti-transferrin receptor (anti-TfR) (Invitrogen) at 1:2,000, anti-GFP (Roche, Indianapolis, IN) at 1:2,000, anti-FLAG M2 (Sigma) at 1:1,000, anti-cyclin D1 Ab-3 (Thermo Scientific, Fremont CA) at 1:1,000, and anti-T7 (Novagen) at 1:5,000. We used the IRDye 800-conjugated goat anti-mouse IgG (Rockland) and the Alexa Fluor 680 goat anti-rabbit IgG (Invitrogen) as secondary antibodies at a 1:10,000 dilution. Proteins were detected using a Li-Cor Odyssey Imaging System and Odyssey, version 2.0, software (Li-Cor, Lincoln, NE).

Live-cell imaging. At 24 h posttransfection, cells were split and plated onto 35-mm dishes fitted with 12-mm glass coverslips (MatTek, Ashland, MA). The following day, medium was replaced with phenol red-free DMEM containing 1 mM sodium pyruvate (Invitrogen) and 10% serum. Live-cell imaging was per-

formed on a Zeiss LSM510 laser scanning confocal system with a Plan-Apochromat 63× (1.4 numerical aperture [63×/1.4]) oil objective. Cerulean images were acquired using the 458-nm laser at 70% transmission along with a 475-nm long-pass filter and 458/514-nm beam splitters. Venus images were acquired using the 514-nm laser at 30% transmission along with a 530-nm long-pass filter and the 458/514-nm beam splitters.

FRAP studies. At 24 h posttransfection NIH 3T3 cells grown on 25-mm coverslips were transferred to live-cell imaging chambers (Atto) in a water-jacketed stage incubator at 37°C. Fluorescence recovery after photobleaching (FRAP) was performed on a Zeiss LSM510 laser scanning confocal system. A 20-μm^2 area was photobleached for 5 s with 100% transmission of the 488-nm argon laser running at 6.3 mW. Fluorescence intensities of the bleached area and a distal unbleached area of equal size were measured every 5 s for 2 min at 20% transmission. Values were normalized to prebleach intensities and compared to the unbleached area to obtain relative fluorescence intensities. Twenty cells per condition were analyzed. The mean time for 50% recovery ($T_{1/2}$) was calculated from recovery curves by nonlinear regression analysis using the equation for one-phase association: $Y = Y_0 + (\text{Plateau} - Y_0) \cdot [1 - \exp(-K \cdot X)]$ (60) using Prism 5 software (GraphPad, La Jolla, CA). Y_0 is the Y value when X (time) is zero; Plateau is the Y value at infinity (∞), K is the rate constant, tau is the time constant ($1/K$), and $T_{1/2} = \ln(2)/K$. Mobility is the difference between Y_0 and Plateau.

Merlin and actin colocalization. SC4 cells were transfected with either Cerulean-merlin WT-Venus or Cerulean-merlin 6N-Venus and plated onto coverslips. Cells were washed in PBS three times, followed by simultaneous fixation and permeabilization in 4% paraformaldehyde containing 0.2% TX-100 for 20 min at room temperature as previously described (33). Coverslips were blocked for 30 min in the dark at room temperature in PBS containing 1% fatty acid-free BSA followed by counterstaining with Alexa Fluor 633-phalloidin at a final concentration of 5U/ml (for actin) and with 4′,6′-diamidino-2-phenylindole (DAPI; for nuclei) for 30 min in the dark at room temperature in blocking buffer. Coverslips were washed, mounted in Biomeda gel mount, and analyzed using a Zeiss LSM710 laser scanning confocal system with a Plan-Apochromat 63×/1.4 oil objective. For cytochalasin D treatment, coverslips were pretreated with 2 μM cytochalasin D for 30 min at 37°C prior to fixation.

Endogenous merlin staining. NIH 3T3 cells or $NF2^{flox2/flox2}$ (carrying two *loxP* sites flanking exon 2) cells plated onto coverslips were washed in PBS and fixed by one of the following methods. For TX-100 extraction prior to fixation, coverslips were incubated with ice-cold 1% TX-100 in PBS for 30 min on ice, washed, and then fixed using 4% paraformaldehyde. For methanol or acetone fixation, coverslips were fixed in 100% methanol or acetone, respectively, for 20 min at −20°C. Following fixation, coverslips were blocked for 1 h at room temperature in PBS containing 5% goat serum and 0.1% BSA. Coverslips were incubated overnight at 4°C with anti-merlin A19 polyclonal primary antibody (1:200 dilution). Coverslips were then incubated with Alexa Fluor 546 goat anti-rabbit secondary antibody (1:500 dilution) and DAPI (1:1,000 dilution) for 1 h at room temperature in the dark. Coverslips were washed, mounted in Biomeda gel mount, and analyzed using a Zeiss LSM710 laser scanning confocal system with a Plan-Apochromat 63×/1.4 oil objective.

Merlin-Venus fluorescence in fixed cells. To visualize merlin-Venus fluorescence in fixed cells, NIH 3T3 cells or SC4 cells transfected with merlin-Venus were plated onto coverslips and fixed using 4% paraformaldehyde following cold 1% TX-100 extraction as described above. Coverslips were then counterstained for nuclei using DAPI (1:1,000 dilution) for 20 min at room temperature in the dark. Coverslips were washed, mounted, and analyzed using a Zeiss LSM710 laser scanning confocal system as described above.

MTT assay. A total of 2.5×10^5 SC4 cells that were plated overnight in four wells of a six-well plate were either infected with recombinant lentivirus or mock infected. After overnight infection, cells were trypsinized, and four 96-well plates were prepared with 2.5×10^3 cells per 100-μl per well, five sets per plate. A total of 2.5×10^5 SC4 infected cells were simultaneously plated in parallel in six-well plates to confirm the expression of recombinant proteins. Methylthiazolyldiphenyl-tetrazolium bromide (MTT) assays were performed daily on one 96-well plate as previously described (35). The readings were corrected with respect to medium alone (blank control).

MEF, adenovirus infection, and BrdU incorporation. The immortalized mouse fibroblastic cell lines $NF2^{flox2/flox2}$ and $NF2^{\Delta 2/\Delta 2}$ were derived from $NF2^{flox2/flox2}$ primary mouse embryonic fibroblasts (MEF) as previously described (5, 35). Cells were infected with the adenovirus indicated on the figures at a multiplicity of infection (MOI) of 250. Cell lysates were analyzed by Western immunoblotting. For bromodeoxyuridine (BrdU) incorporation, cells infected with the adenovirus indicated on the figures on 22-mm^2 coverslips were incubated with 10 μM BrdU (BrdU kit 1; Roche) for 1 h at 37°C and analyzed as per the manufacturer's instructions. BrdU immunofluorescence was detected using goat-anti-mouse Alexa Fluor 546 at 1:200, and nuclei were counterstained with DAPI (Molecular probes). At least 500 cells per field (10 fields per coverslip) were counted in two independent experiments each.

Adhesion assay. $NF2^{\Delta 2/\Delta 2}$ cells were infected with the adenovirus indicated on the figures at an MOI of 250. Confluent cells were either left in regular (10% FBS) medium or serum starved in DMEM (0% FBS) for 24 h. For suspension analysis, one set of serum-starved cells was washed twice with Hanks' balanced salt solution (HBSS), trypsinized, washed twice in DMEM containing 0.1% soya bean trypsin inhibitor and 0.1% essentially fatty acid-free BSA, and finally resuspended in DMEM for 30 min at 37°C as previously described (55).

Colony formation assay. SC4 cells were transfected with pCDH constructs containing a puromycin resistance gene. Forty-eight hours posttransfection, 3×10^4 cells of each type were plated in triplicate in 10-cm dishes and selected with 3 μg/ml puromycin for a week. Medium was changed every 2 to 3 days. Untransfected cells were completely dead within 3 to 4 days (data not shown). Colonies were stained with crystal violet.

RESULTS

Merlin FERM domain binds phosphoinositides. Comparison with the ezrin sequence reveals that potential PIP_2 binding motifs [KKX_n(K/R)K] are present in the FERM domain of human merlin (Fig. 1A) at 79-KKVLDHDVSK-88 and at 269-KEFTIKPLDKK-279. To test the hypothesis that these motifs are involved in PIP_2 binding, we converted the homologous charged residues K79, K80, K269, E270, K278, and K279 to neutral asparagines (merlin 6N). Wild-type merlin and merlin 6N FERM domains fused to GST were tested for lipid binding. The FERM domain of wild-type merlin binds phosphorylated phosphoinositides including PIP_2 (Fig. 1Be), whereas the merlin 6N FERM domain shows drastically reduced binding (Fig. 1Bf). These results were confirmed using PIP arrays (Fig. 1C). Thus, the merlin FERM domain binds phosphorylated phosphoinositides *in vitro*, and the charged amino acids K79, K80, K269, E270, K278, and K279 are necessary for this interaction.

Mutant merlin is folded properly. To exclude the possibility that introduction of the six point mutations in the FERM domain of merlin drastically alters the folding of FERM domain or full-length merlin, we performed the following experiments. The overall intrinsic tryptophan fluorescence profiles of GST-FERM WT and GST-FERM 6N were recorded. They are very similar without significant changes in either the maximum intensity of fluorescence or the wavelength of maximum emission (Fig. 2A). Similarly, the digestion patterns of GST-FERM domain proteins (WT and 6N) following limited chymotryptic proteolysis are similar (Fig. 2B). To investigate for changes in full-length merlin conformation upon introduction of the 6N mutations, we performed FRET spectrofluorometry as previously described (22). The emission spectra of Cerulean-merlin WT-Venus and Cerulean-merlin 6N-Venus proteins are similar, indicating that both the wild-type and 6N mutant merlin proteins adopt similar conformations. Treatment with 0.1% SDS, which denatures merlin, served as an internal negative control (Fig. 2C). Full-length Cerulean-merlin-Venus wild-type and 6N merlin secondary structure content was compared by far-UV CD spectroscopy to verify that the mutant had folded with a backbone conformation similar to that of wild-type merlin (Fig. 2D). The spectra are similar, indicating an overall similar fold, but the minor deviations between 213 and 227 nm indicate slight differences in α-helical content. This is confirmed by the CDSSTR deconvolution, which shows an average difference of about 6% helix and sheet content be-

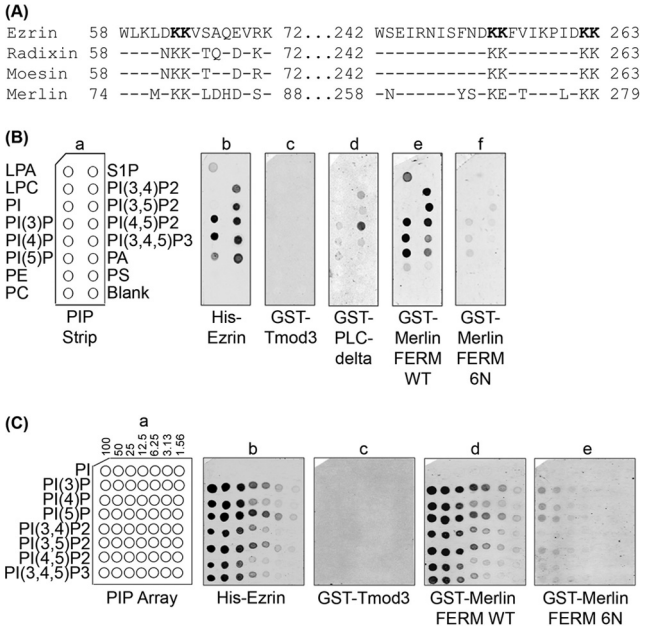

FIG. 1. Merlin FERM domain binds phosphoinositides. (A) Sequence alignment of the parts of the FERM domains of ezrin, radixin, moesin, and merlin that contain the PIP_2 binding motif. The residues involved in PIP_2 binding in ezrin (3) are shown in bold type. (B) Protein-lipid overlay assay using PIP strips containing 100 picomoles per spot of various phosphoinositides and lipids ($n \geq 3$). Compared to GST-merlin FERM WT, the GST-merlin FERM 6N shows greatly reduced binding to phosphorylated phosphoinositides. Panels b and d are positive controls for PIP binding. GST-tropomodulin 3 (GST-Tmod3), an actin binding protein that does not bind PIP, is a negative control. GST alone does not bind PIP (data not shown). LPA, lysophosphatidic acid; LPC, lysophosphocholine; PI, phosphatidylinositol; PI(3)P, phosphatidylinositol-3-phosphate; PI(4)P, phosphatidylinositol-4 phosphate; PI(5)P, phosphatidylinositol-5-phosphate; PE, phosphatidylethanolamine; PC, phosphatidylcholine; S1P, sphingosine-1 phosphate; $PI(3,4)P_2$, phosphatidylinositol-3,4-bisphosphate; $PI(3,5)P_2$, phosphatidylinositol-3,5-bisphosphate; $PI(4,5)P_2$, phosphatidylinositol-4,5-bisphosphate; $PI(3,4,5)P_3$, phosphatidylinositol-3,4,5-trisphosphate; PA, phosphatidic acid; PS, phosphatidylserine. (C) Protein-lipid overlay assay using PIP array containing concentration gradients (1.5 picomoles to 100 picomoles) of various phosphoinositides ($n = 3$). His-ezrin and GST-merlin FERM WT bind phosphorylated phosphoinositides including PIP_2 but not the unphosphorylated phosphoinositide, PI (top row). GST-merlin FERM 6N shows significantly decreased binding to phosphoinositides. GST-Tmod3 (negative control) shows no binding to phosphoinositides, and GST-PLC-δ binds PIP_2 (data not shown).

tween the wild-type and mutant proteins. Specifically, the mutant protein showed a 4 to 9% increase in α-helix in conjunction with a 4 to 7% decrease in β-strand content. Minor (~1%) shifts in turn and coil content were also observed between the wild-type and mutant proteins. Additionally, no significant differences were observed in AUC experiments comparing the wild-type and mutant 6N proteins (Fig. 2E). The slight decrease in sedimentation coefficient (s^*) observed for the mutant 6N protein (5.4 ± 0.8) is still within error of the wild-type protein (5.5 ± 0.7). If the 6N mutations led to a large-scale unfolding of the mutant, we would expect an increased frictional ratio (f/f_0) relative to the wild type, but this is not the case as the frictional ratio is 1.6 for both the wild type and 6N mutant. The molecular mass of Cerulean-merlin 6N-Venus was calculated to be 124 ± 31 kDa versus 125 ± 30 kDa for Cerulean-merlin WT-Venus, which is in close agreement with its calculated molecular mass of 130 kDa. Thus, both the sedimentation coefficient and frictional ratio values are consistent with similar sizes and shapes of wild-type and 6N mutant merlin proteins, indicating that the mutations do not cause any large-scale structural perturbations. Furthermore, GST–NHE-RF pulldown reveals that both full-length merlin WT-GFP and full-length merlin 6N-GFP bind to GST–NHE-RF, a known merlin binding partner (Fig. 2F). Taken together, these studies indicate that the introduction of six amino acid point mutations in the PIP binding motif within the merlin FERM domain does not drastically alter the structure of either the FERM domain or that of full-length merlin.

PIP binding of the merlin FERM domain is essential for its association with cholesterol-dependent membrane domains. We have previously shown that exogenously expressed merlin-GFP resides in the cholesterol-dependent 20% and 25% fractions following density gradient centrifugation (61). We verified that endogenous merlin from confluent $NF2^{flox2/flox2}$ MEF cells also equilibrates to the same buoyant fractions (Fig. 3A). Importantly, pretreatment with 10 mM methyl-β-cyclodextrin (MβCD; a cholesterol-extracting reagent) for 30 min results in the disappearance of merlin from the 20% fraction and a decrease in the amount of merlin in the 25% fraction, indicating that the 20% and 25% fractions represent cholesterol-dependent domain fractions. MβCD treatment results in a similar shift of caveolin, a protein known to reside in cholesterol-dependent membrane domains, to higher-density fractions without affecting the fractionation of the negative-control marker, transferrin receptor (TfR).

To determine if PIP_2 binding plays a role in the association of merlin with membrane domains, we performed two types of assays: solubility in cold nonionic detergent and density gradient centrifugation. In the first, lysates from confluent NIH 3T3 cells (a condition that activates the growth-suppressive function of merlin) expressing empty vector or T7-tagged merlin WT FERM or merlin 6N FERM were sequentially extracted with cold 1% TX-100 and 100 mM NOG. As reviewed by Shogomori and Brown (59), insolubility of a protein in TX-100 and its solubility in NOG are good indicators that the protein resides in cholesterol-dependent membrane domains. The wild-type merlin FERM domain is present in both the TX-100-soluble and the TX-100-insoluble–NOG-soluble fractions (Fig. 3B). In contrast, the merlin 6N FERM domain, which does not bind PIP, resides almost exclusively in the TX-100-soluble fraction and is essentially absent in the TX-100-insoluble–NOG-soluble fraction.

A more definitive indication for cholesterol-dependent membrane domain residence is the buoyancy of the candidate in a density gradient (18, 20, 64). Similar to full-length endogenous merlin (Fig. 3A), the T7-tagged wild-type merlin FERM domain equilibrates to the 20% and 25% fractions of the density gradient (Fig. 3C). In contrast, the T7-tagged merlin 6N FERM domain, which does not bind PIP, is mainly present in the higher-density fractions (Fig. 3C).

This conclusion was confirmed by a more detailed analysis in which PIP binding mutations were studied in the context of full-length merlin. In this analysis, two (K79 and K80; merlin 2N), four (K79, K80, K269, and E270; merlin 4N), or all six

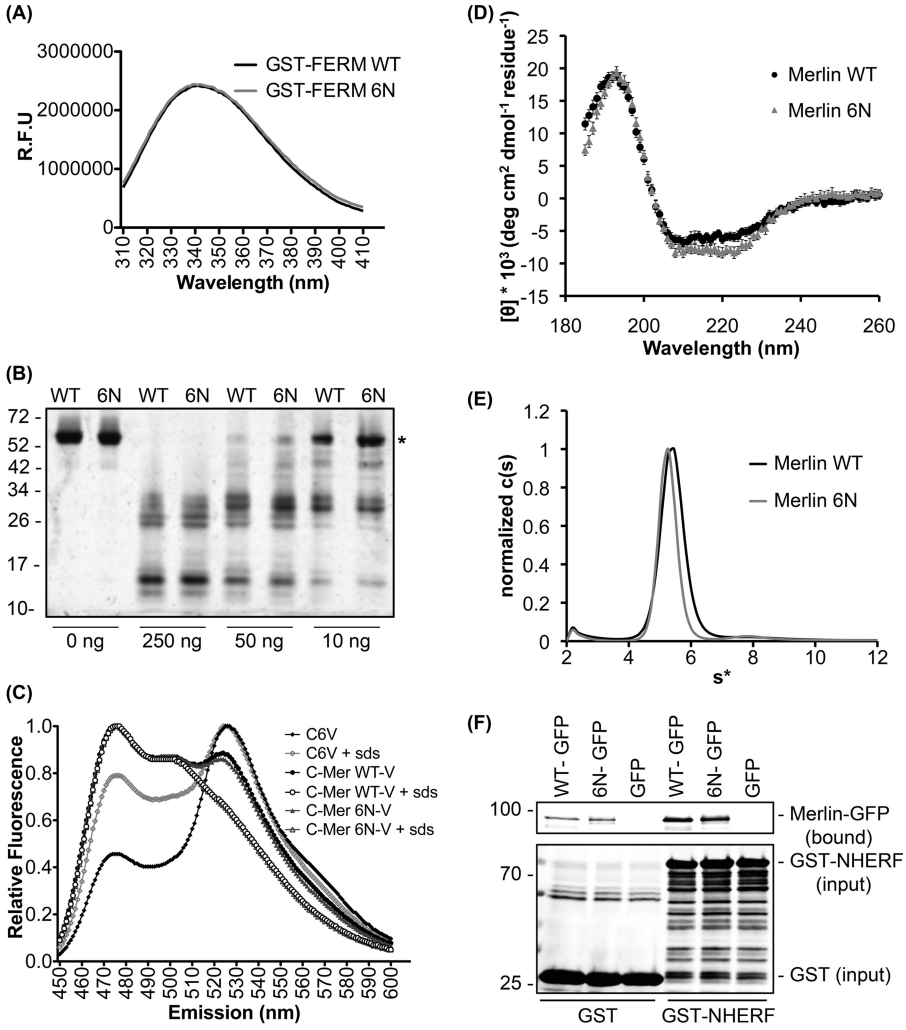

FIG. 2. Mutant merlin 6N is properly folded. (A) Tryptophan fluorescence. GST-FERM WT and 6N proteins have similar tryptophan fluorescence profiles following excitation at 295 nm ($n = 3$). The y axis shows the relative fluorescence units at the different wavelengths (x axis). (B) Chymotryptic digest. Coomassie-stained gel shows that both GST-FERM WT and GST-FERM 6N proteins yield similar-size peptide fragments with various concentrations of chymotrypsin. The asterisk denotes the position of uncleaved GST-FERM proteins. (C) FRET spectrofluorometry. Mean emission spectra of full-length purified proteins following excitation at 435 nm and measured in triplicate at room temperature are plotted, normalized to the maximum value in each given scan such that all plotted values are ≤1. FRET (the fluorescence emission of acceptor Venus between 515 nm and 550 nm when excited at the donor Cerulean excitation wavelength of 435 nm) is not significantly different between Cerulean-merlin WT-Venus (C-Mer WT-V) and Cerulean-merlin 6N-Venus (C-Mer 6N-V). Addition of 0.1% SDS (internal negative control) abolishes the FRET for both WT and 6N proteins, indicating that FRET requires properly folded merlin. FRET of C6V (positive control) is not affected by 0.1% SDS as previously shown (22). Cerulean alone (negative control) did not show FRET (data not shown), as described previously (22). (D) Circular dichroism. Full-length merlin WT and mutant merlin 6N (C-Mer-V) secondary structure contents were compared by far-UV CD spectroscopy. The spectra are similar, indicating overall similar folds. The y axis shows the mean residue ellipticity (see Materials and Methods). (E) Analytical ultracentrifugation. AUC studies of purified full-length (WT and 6N) C-Mer-V show that the sedimentation coefficient values (5.5 ± 0.7 versus 5.4 ± 0.8) and apparent molecular masses (125 ± 30 kDa versus 124 ± 31 kDa) are not significantly different between the WT and 6N proteins. Values in parenthesis are for WT and 6N, respectively. The frictional ratios (f/f_0) are also identical (1.6) for both proteins. (F) GST—NHE-RF pulldown. Merlin WT and mutant merlin 6N bind NHE-RF. Lysates from SC4 cells transfected with full-length merlin WT-GFP, merlin 6N-GFP, or GFP alone were subjected to GST or GST–NHE-RF pulldown as described in Materials and Methods.

(K79, K80, K269, E270, K278, and K279; merlin 6N) putative PIP binding residues were altered in full-length merlin. Mutating the FERM domain PIP binding sites similarly decreases the amount of merlin in the TX-100-insoluble–NOG-soluble fraction (data not shown). As shown previously (61), full-length FLAG-tagged WT merlin is present in the low-density 20% and 25% fractions (Fig. 3D) in a cholesterol-dependent manner (similar to Fig. 3A) (data not shown). In contrast, full-length merlin 2N showed decreased flotation to the 20% fraction and a shift toward the higher-density fractions. Full-length merlin 4N showed the same tendency but to a greater extent, whereas full-length merlin 6N was almost completely excluded from the 20% and 25% fractions and was present predominantly in the higher-density fractions. Approximately 50% of total full-length WT merlin associates with the cholesterol-dependent 20% and 25% fractions, which significantly

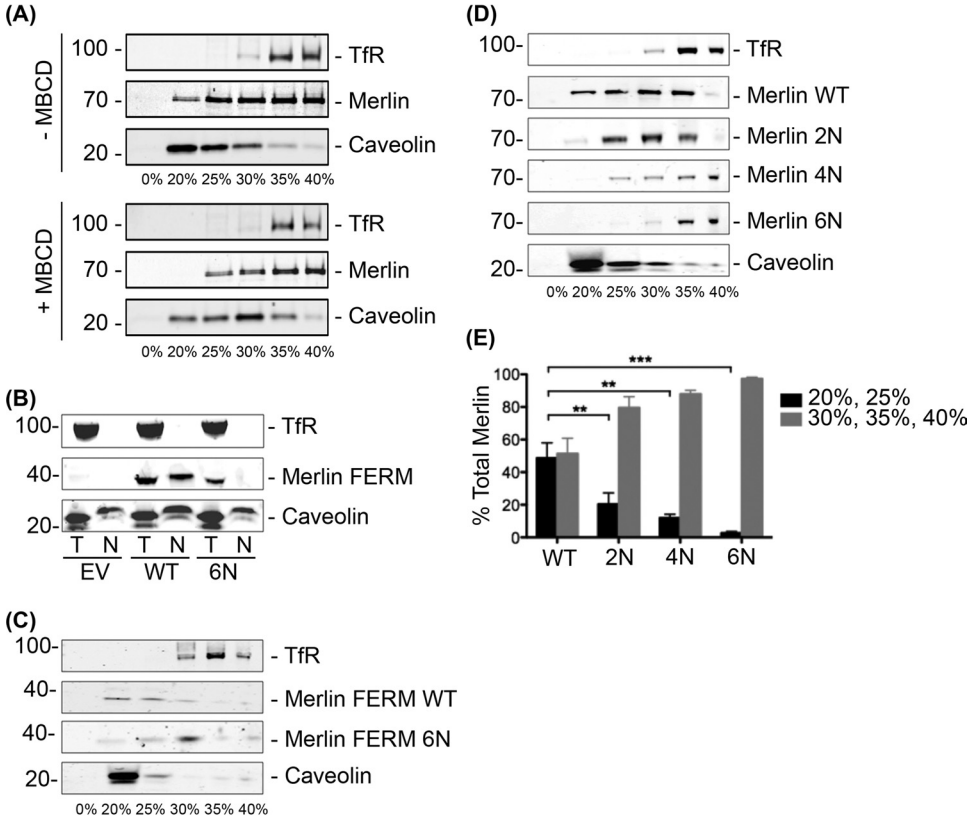

FIG. 3. FERM domain PIP binding regulates the association of merlin with cholesterol-dependent membrane domains. (A) Endogenous merlin resides in cholesterol-dependent buoyant fractions. Confluent $NF2^{flox2/flox2}$ MEF cells were pretreated with either DMEM or 10 mM MβCD (methyl-β-cyclodextrin, a cholesterol-extracting reagent) in DMEM for 30 min at 37°C prior to cell lysis. Western immunoblotting following density gradient centrifugation of whole-cell lysates shows that endogenous merlin is present in the buoyant fractions (20% and 25%). Transferrin receptor (TfR) and caveolin are shown as controls. MβCD treatment results in the disappearance of merlin from the 20% fraction and a decrease in the amount of merlin in the 25% fraction, indicating that the 20% and 25% fractions are cholesterol dependent. MβCD treatment similarly results in a shift of caveolin to the higher-density fractions without affecting the fractionation of the negative-control marker, transferrin receptor (TfR). (B) T7-tagged merlin FERM WT is present in both the TX-100 soluble (T) and the TX-100-insoluble–NOG-soluble (N) fraction, whereas the level of T7-tagged merlin FERM 6N mutant in the TX-100-insoluble–NOG-soluble fraction is drastically reduced in transfected NIH 3T3 cells. Transferrin receptor is a control for the TX-100-soluble fraction, and caveolin, a known component of membrane domains, is present in both the TX-100-soluble and the TX-100-insoluble–NOG-soluble fractions. Results in panels A and B are representative of three independent experiments. EV, empty vector. (C) OptiPrep fractionation of whole-cell lysates from confluent and transfected NIH 3T3 cells shows that T7-tagged merlin FERM WT is present in the 20% and 25% fractions of the density gradient, whereas the T7-tagged merlin FERM 6N is mainly present in the higher-density fractions. (D) OptiPrep fractionation of lysates from confluent and transfected NIH 3T3 cells ($n \geq 3$) shows that FLAG-tagged full-length WT merlin floats to the buoyant fractions (20% and 25%) of the density gradient. Transferrin receptor and caveolin are shown as controls. FLAG-tagged full-length merlin 2N and 4N show decreased flotation to the 20% fraction. FLAG-tagged full-length merlin 6N is excluded from the 20% and 25% fractions altogether and is mainly present in the higher-density fractions. We probed for the transferrin receptor and caveolin in each case (data not shown). Similar results were also obtained in SC4 cells (Fig. 9 and data not shown). (E) Quantification of density gradient centrifugation for FLAG-tagged full-length merlin using Odyssey, version 2.0, software shows decreasing residence in the cholesterol-dependent buoyant fractions (20% and 25%) and a corresponding increase in the higher-density fractions (30%, 35%, and 40%) as the PIP_2 binding motif in the FERM domain is progressively modified. Statistical analysis was performed using two-way analysis of variance. Error bars indicate means + standard errors of the means. **, $P < 0.01$; ***, $P < 0.001$.

decreases with progressive ablation of the PIP binding sites (Fig. 3E). Thus, for both the merlin FERM domain alone and the full-length merlin molecule, PIP binding to the FERM domain regulates its detergent resistance and its association with cholesterol-dependent membrane domains.

FERM domain PIP binding regulates subcellular localization of merlin. The results presented above suggest that FERM domain PIP binding may affect the subcellular localization of merlin. To assess this possibility, we constructed expression vectors by fusing two variants of GFP in frame to either the amino or carboxy terminus of merlin as previously described (22). Cerulean is a monomeric, blue-shifted GFP (53), whereas Venus is yellow shifted (46). The following vectors were created: Cerulean-merlin WT, merlin WT-Venus, Cerulean-merlin WT-Venus, and their PIP binding-deficient counterparts.

Confocal imaging of live, transfected NIH 3T3 cells showed that WT merlin is predominantly localized to regions of the plasma membrane and cell periphery irrespective of the location of the modified GFP tag (Fig. 4A). In addition, WT merlin was also present at regions of the cell-cell boundary (Fig. 4Ae). Cerulean-merlin 2N-Venus had a subcellular localization similar to that of WT merlin but was also present at a low but

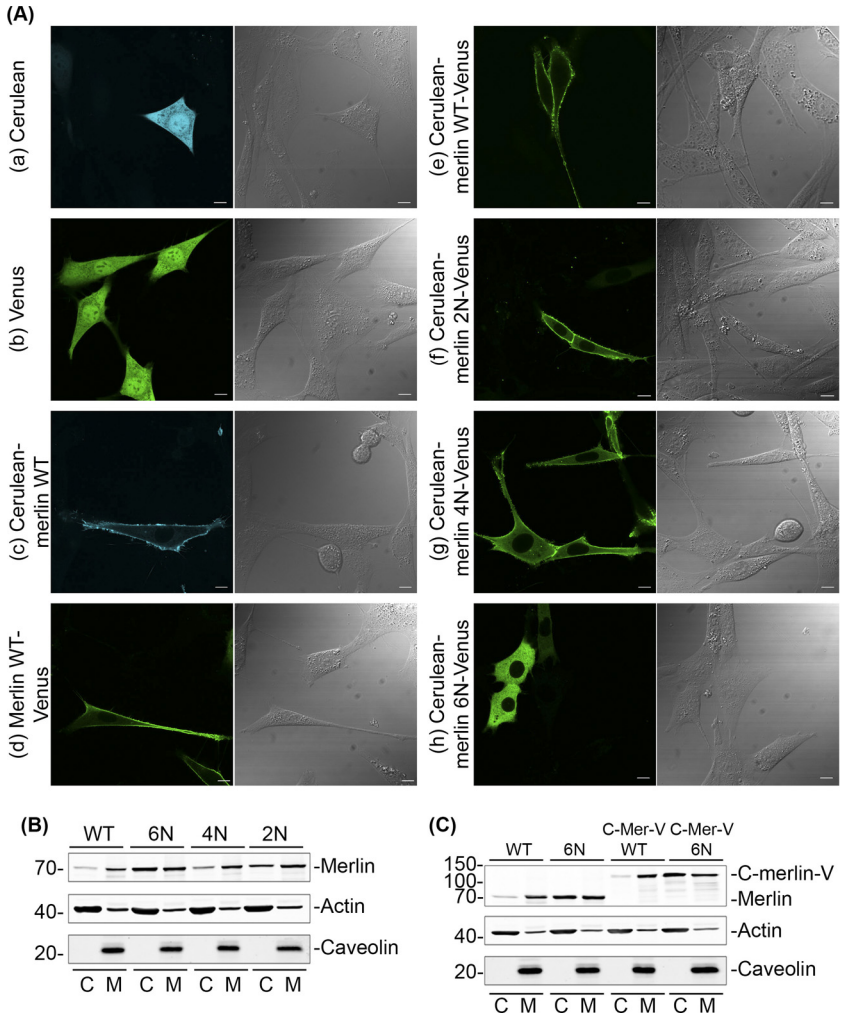

FIG. 4. FERM domain PIP binding regulates subcellular localization of merlin. (A) By confocal live microscopy, NIH 3T3 cells expressing Cerulean alone (a) or Venus alone (b) showed uniform and diffuse fluorescence throughout the cytoplasm and nucleus. WT merlin is predominantly localized to regions of the plasma membrane irrespective of whether the modified GFP tag is present at the amino terminus (Cerulean-merlin WT), the carboxy terminus (Merlin WT-Venus), or at both termini (Cerulean-merlin WT-Venus). Additionally, WT merlin is also present at regions of the cell-cell boundary (e). Merlin 2N (Cerulean-merlin 2N-Venus) and merlin 4N (Cerulean-merlin 4N-Venus) are localized to the plasma membrane and regions of the cell-cell boundary but are also detectable in the cytoplasm. In contrast, merlin 6N (Cerulean-merlin 6N-Venus) shows predominantly cytoplasmic localization and is not enriched at regions of the cell-cell boundary. Corresponding differential interference contrast images are shown in the right panels. Scale bar, 10 μm. (B and C) Confluent NIH 3T3 cells expressing the indicated merlin constructs were fractionated into cytosolic (C) and membrane (M) fractions and analyzed by immunoblotting. Full-length FLAG-tagged WT merlin is mainly present in the membrane fractions. Mutating the FERM domain PIP binding sites increases the amount of mutant merlin in the cytosolic fractions. The efficiency of fractionation was verified using caveolin as a membrane marker, and actin was used as a loading control for corresponding lanes (B). The Cerulean-merlin-Venus fusion proteins (WT and 6N) fractionate similarly to their respective non-GFP-tagged merlin proteins (C).

detectable level in the cytoplasm (Fig. 4Af). Similarly, merlin 4N localized to the plasma membrane and regions of the cell-cell boundary but also the cytoplasm (Fig. 4Ag). In contrast, merlin 6N, which does not bind PIP at its FERM domain, showed predominantly cytoplasmic localization and is not enriched at regions of the cell periphery or cell-cell boundary (Fig. 4Ah). Similar live-cell imaging results were obtained in transfected SC4 cells (data not shown).

The results of subcellular localization were verified by biochemical fractionation. Whereas WT merlin is predominantly present in the membrane fraction, mutating the FERM domain PIP binding sites significantly increases the amount of mutant merlin in the cytosolic fractions (Fig. 4B). To rule out the possibility that the addition of GFP tags to merlin alters its localization, we compared the fractionation of merlin with or without the GFP tags. Both of the Cerulean-merlin-Venus fusion proteins, WT and 6N, fractionated similarly to the respective non-GFP tagged merlin proteins, with the PIP binding mutants localizing more to the cytosolic fractions than their WT counterparts (Fig. 4C).

Confocal imaging of endogenous merlin staining after extraction with ice-cold 1% TX-100 followed by 4% paraformaldehyde fixation in both NIH 3T3 cells and in $NF2^{flox2/flox2}$ MEF cells revealed a distinct punctate membrane localization,

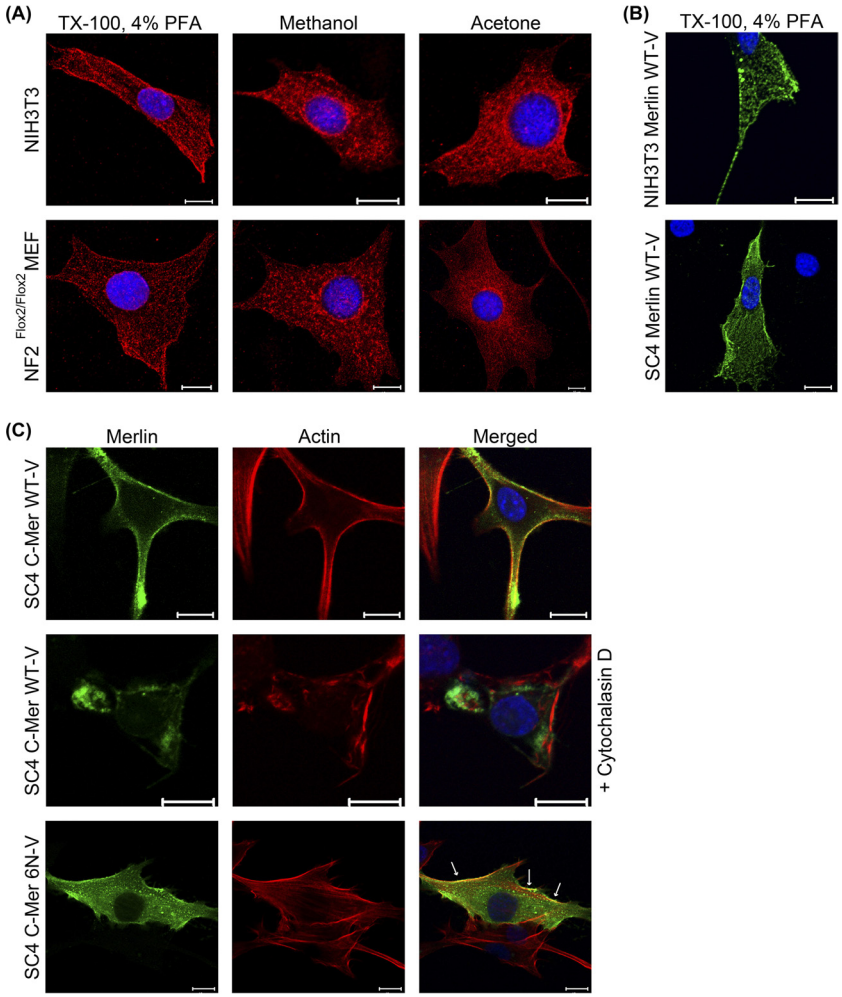

FIG. 5. Subcellular localization of endogenous or transfected merlin in fixed cells. (A) Confocal images of NIH 3T3 cells and $NF2^{flox2/flox2}$ MEF cells that were fixed either with 4% paraformaldehyde after ice-cold 1% TX-100 extraction (TX-100, 4% PFA), methanol, or acetone reveal that endogenous merlin shows a distinct punctate membrane localization. Merlin is shown in red, and nuclei are in blue (DAPI). (B) Confocal images of NIH 3T3 cells or SC4 cells transfected with merlin WT-Venus and fixed with 4% paraformaldehyde after ice-cold 1% TX-100 extraction (TX-100, 4% PFA) similarly reveal a distinct punctate membrane fluorescence. Merlin-Venus fluorescence is shown in green, and nuclei are in blue (DAPI). (C) Confocal images of SC4 cells transfected with Cerulean-merlin-Venus following fixation and permeabilization in 4% paraformaldehyde containing 0.2% TX-100 and counterstaining with phalloidin (for actin) are shown. The top row shows that merlin WT (green) shows extensive colocalization (yellow) with actin (red). Pretreatment with cytochalasin D, which disrupts actin cytoskeleton, results in the loss of this colocalization and accumulation of merlin as intracellular aggregates (middle row). The bottom row shows that merlin 6N was largely cytoplasmic (green) where it did not colocalize with actin (red). However, some of the merlin 6N fluorescence that does remain at the membrane did colocalize (yellow) with actin (arrows).

as described previously (10, 61). Similar endogenous merlin staining was observed following methanol or acetone fixation in NIH 3T3 cells and in $NF2^{flox2/flox2}$ cells (Fig. 5A). To directly compare this localization of endogenous merlin with that of fluorescence from the modified GFP fused to merlin (Fig. 4 shows live-cell imaging), we analyzed the localization of merlin WT-Venus fluorescence in NIH 3T3 cells and SC4 cells after extraction with ice-cold 1% TX-100 followed by 4% paraformaldehyde fixation. Fixation under this condition revealed a distinct punctate membrane merlin WT-Venus fluorescence in both NIH 3T3 cells and in SC4 cells (Fig. 5B), similar to that of endogenous merlin in NIH 3T3 cells and in $NF2^{flox2/flox2}$ cells. Thus, both endogenous and overexpressed epitope-tagged merlin proteins appear in the same subcellular compartment.

Next, we wished to determine whether FERM domain-mediated PIP binding and subsequent membrane association are required for merlin colocalization with the actin cortical cytoskeleton. In SC4 cells transfected with Cerulean-merlin-Venus (WT and 6N), merlin WT fluorescence localized to the cortical membrane and colocalized with phalloidin (actin) staining. This colocalization was dependent on intact actin cytoskeleton/cellular architecture as treatment with cytochalasin D resulted in loss of merlin WT and actin colocalization and accumulation of merlin WT as large aggregates, as previously described (10, 33). In contrast, merlin 6N fluorescence was largely cytoplas-

mic (Fig. 5C). However, some of the merlin 6N fluorescence that does remain at the membrane (Fig. 4C) colocalized with actin (see discussion below).

FERM domain PIP binding regulates merlin dynamics. To determine if PIP binding regulates merlin localization dynamically, we assessed the mobility of the expressed merlin in live transfected NIH 3T3 cells by fluorescence recovery after photobleaching (FRAP). Venus was used as a freely diffusible protein control, and GFP fused in frame with histone 2B (H2B-GFP) was used as a control for an essentially immobile protein (2, 50).

The $T_{1/2}$ of recovery for wild-type Cerulean-merlin WT-Venus suggests that merlin is not freely diffusible but likely tethered to structural elements in the cell. In stark contrast, the FRAP behavior of the PIP binding-deficient merlin (merlin 6N) was essentially identical to that of the freely diffusible Venus (Fig. 6). Finally, the recovery of fluorescence in cells transfected with Cerulean-6-Venus (Cerulean and Venus fused in frame and separated by a 6-residue linker) was identical to that of cells transfected with Venus alone, indicating that the presence of two modified GFPs does not alter FRAP under these experimental conditions (data not shown).

FERM domain PIP binding is not required to regulate merlin phosphorylation at S518. For ezrin, phosphorylation is regulated by FERM domain PIP_2 binding (3, 14). As merlin is regulated by phosphorylation at S518 (56), we analyzed cell lysates from $NF2^{\Delta 2/\Delta 2}$ MEF cells following reexpression of wild-type or mutant merlin proteins for their steady-state S518 phosphorylation status. Interestingly, we found that FERM domain PIP binding is not required for steady-state S518 phosphorylation in $NF2^{\Delta 2/\Delta 2}$ MEF cells (Fig. 7A) and in NIH 3T3 cells and SC4 cells (data not shown).

We further examined if the 6N mutation affected the phosphorylation status of merlin in response to loss of adhesion. We found that both merlin WT and 6N can be dephosphorylated at S518 following simultaneous serum starvation and suspension (Fig. 7B), as previously described (55). In addition, both merlin WT and 6N can be further phosphorylated at S518 by cotransfection with active Rac Q61L (Fig. 7C), as previously described (29, 56). These results suggest that FERM domain PIP binding is not required to significantly regulate merlin phosphorylation at S518.

FERM domain PIP binding is essential for the growth-suppressive function of merlin. Reexpression of merlin in SC4 cells inhibits cell growth (45). To determine if FERM domain PIP binding regulates the growth-suppressive function of merlin, SC4 cells were either infected with recombinant lentivirus expressing full-length WT merlin or full-length merlin 6N or GFP or mock infected. SC4 cells infected with full-length WT merlin had a significantly reduced growth rate on days 3 and 4 compared to that of the controls (Fig. 8A). In contrast, SC4 cells infected with full-length merlin 6N grew at the same rate as mock-infected and control GFP-infected cells.

Several studies have shown that merlin inhibits cell proliferation and cell cycle progression, at least in part by repressing cyclin D1 expression (5, 10, 26, 31, 48, 67). Reexpression of WT merlin in merlin-null $NF2^{\Delta 2/\Delta 2}$ MEF and in merlin-null SC4 cells (data not shown) is sufficient to repress cyclin D1 expression. In contrast, the mutant merlin 6N does not repress cyclin D1 expression (Fig. 8B). Consistent with this result, reexpression of WT merlin, but not mutant merlin 6N or the GFP control, in merlin-null $NF2^{\Delta 2/\Delta 2}$ MEF inhibits cell proliferation as assessed by BrdU incorporation (Fig. 8C). Additionally, reexpression of WT merlin, but not of mutant merlin 6N, was sufficient to significantly inhibit colony formation compared to vector alone in SC4 cells following puromycin selection (Fig. 8D). Taken together, these results indicate that in the absence of FERM domain PIP binding, the ability of merlin to suppress cell growth is significantly compromised. Finally, it has been reported recently that merlin inhibits phospho-S6, phospho-S6 kinase (S6K), and mTOR signaling (26, 40). In our hands, mutant merlin 6N inhibits phospho-S6 and phospho-S6K as efficiently as WT merlin, indicating that FERM domain phosphoinositide binding is not a prerequisite for inhibition of mTOR signaling by merlin (data not shown).

Retargeting the FERM domain PIP binding-deficient mutant merlin into the membrane is sufficient to restore the growth-suppressive function to the mutant merlin. To test if retargeting of the mutant merlin 6N to the membrane is sufficient to rescue its growth-suppressive defect, we fused the first 10 amino acids from the Src family kinase Fyn (Fyn_{1-10}) to its amino terminus. Fyn_{1-10} is myristoylated at glycine-2 and palmitoylated at cysteine-3. This dual acylation confers a high affinity for signaling-rich membrane domains that have high cholesterol and glycosphingolipid contents (38, 52, 68). In a density gradient, Fyn_{1-10} is sufficient to target GFP, as well as retarget the mutant merlin 6N, into the buoyant 20% and 25% fractions following ultracentrifugation (Fig. 9A), confirming its ability to restore proper localization to the mutant merlin 6N. Importantly, Fyn_{1-10}-merlin 6N is sufficient to significantly inhibit colony formation of SC4 cells to the level of wild-type merlin (Fig. 9B). Thus, retargeting of the FERM domain PIP binding-deficient merlin into the membrane is sufficient to restore growth-suppressive properties to the mutant merlin.

DISCUSSION

Recent studies have provided strong evidence that merlin must be at or near the plasma membrane for it to function as a growth regulator (10, 11, 31–33, 41, 43). While details of how merlin functions at the membrane appear to differ between cell types and species, merlin regulates the availability of growth factor receptors either by affecting the rate at which they are internalized or by sequestering them in inert compartments where they cannot signal (43). In addition, merlin regulates the delivery to and the accumulation of growth factor receptors at the plasma membrane (32).

How merlin associates with the membrane, however, is less clear. Since it is not an integral membrane protein, its association with the membrane must be mediated by an intermediary protein or a resident phospholipid. In this paper, we report that phosphoinositide binding tethers merlin to the plasma membrane. Importantly, this binding is necessary for its growth-suppressive function.

The residues implicated in FERM domain-mediated PIP_2 binding are conserved among the ERM proteins and are located at the surface of the molecule, a positively charged flat surface formed by subdomains A and C and containing a basic cleft (17, 36). Likewise, the corresponding surface of the merlin FERM domain is positively charged, suggesting that a sim-

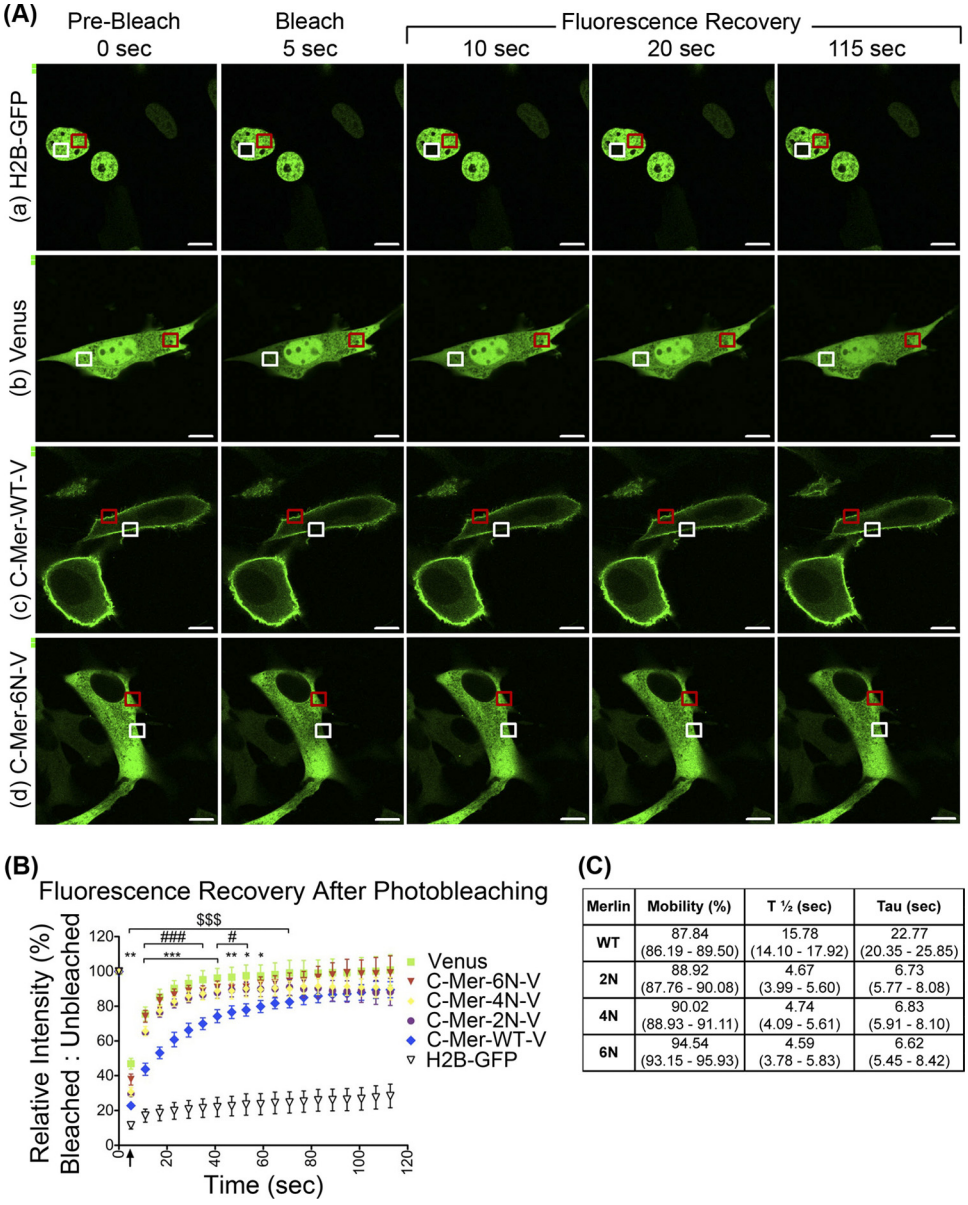

(C)

Merlin	Mobility (%)	T ½ (sec)	Tau (sec)
WT	87.84 (86.19 - 89.50)	15.78 (14.10 - 17.92)	22.77 (20.35 - 25.85)
2N	88.92 (87.76 - 90.08)	4.67 (3.99 - 5.60)	6.73 (5.77 - 8.08)
4N	90.02 (88.93 - 91.11)	4.74 (4.09 - 5.61)	6.83 (5.91 - 8.10)
6N	94.54 (93.15 - 95.93)	4.59 (3.78 - 5.83)	6.62 (5.45 - 8.42)

FIG. 6. FERM domain PIP binding regulates merlin dynamics. (A) Representative confocal images showing fluorescence recovery after photobleaching in NIH 3T3 cells ($n = 20$) transfected with H2B-GFP (a), Venus (b), Cerulean-merlin WT-Venus (c), and Cerulean-merlin 6N-Venus (d). Cells transfected with Cerulean-merlin 2N-Venus and Cerulean-merlin 4N-Venus had similar recovery as those transfected with Cerulean-merlin 6N-Venus (data not shown). A 20-μm^2 area was photobleached (white box) for 5 s, and the recovery of fluorescence in this area was measured every 5 s for 2 min along with the fluorescence in a control nonbleached 20-μm^2 area in the cell (red box). Scale bar, 10 μm. (B) Quantification of FRAP analysis. The normalized relative fluorescence intensities (bleached versus unbleached) were plotted as a percentage on the y axis with time in seconds on the x axis. Cells transfected with Venus alone (green; positive control) had a quick recovery consistent with it being freely diffusible. Cells transfected with H2B-GFP, an essentially immobile protein, failed to recover fluorescence efficiently (black; negative control). The fluorescence recovery of cells transfected with Cerulean-merlin WT-Venus (blue) was significantly slower ($$$, $P < 0.001$) than that of cells transfected with Venus alone. FRAP in cells transfected with Cerulean-merlin 2N-Venus (purple) or Cerulean-merlin 4N-Venus (yellow) (###, $P < 0.001$; #, $P < 0.05$) or with Cerulean-merlin 6N-Venus (red; ***, $P < 0.001$; **, $P < 0.01$; *, $P < 0.05$) was significantly faster than with Cerulean-merlin WT-Venus and was essentially identical to that of freely diffusible Venus. Two-way analysis of variance was used for statistical analysis. Error bars indicate the means ±95% confidence intervals. (C) Table showing the mean percentages of the mobile fraction, the $T_{1/2}$ of recovery, and tau calculated using the equation described in Materials and Methods. Values in parentheses denote 95% confidence intervals. Note that the merlin mutants have a significantly shorter $T_{1/2}$ and tau values than WT merlin.

ilar interaction of these residues with the negatively charged phospholipids, such as PIP_2 molecules in the bilayer, is feasible (58). Although our *in vitro* studies show that merlin binds many PIPs, it is likely that in quiescent cells PIP_2 is the physiological PIP that binds merlin and targets it to the membrane. PIP_2 and phosphatidyl inositol-3,4,5-triphosphate [$PI(3,4,5)P_3$] are the major species at the plasma membrane (13), but PIP_2, at ~10% of total PIP, is far more abundant than $PI(3,4,5)P_3$ since

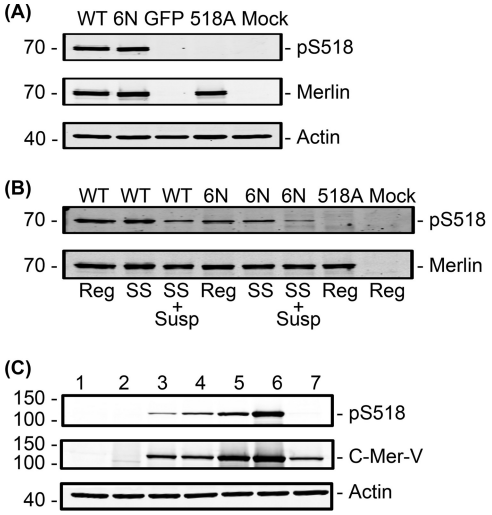

FIG. 7. FERM domain PIP binding is not required to regulate merlin phosphorylation at S518. (A) FERM domain PIP binding is not required for steady-state S518 phosphorylation. $NF2^{\Delta 2/\Delta 2}$ MEF cells were infected with the indicated adenovirus, and lysates were run for Western immunoblotting. (B) WT and 6N merlin can be dephosphorylated at S518 following simultaneous serum starvation and suspension. $NF2^{\Delta 2/\Delta 2}$ MEF cells infected with the indicated adenovirus were either left in 10% FBS regular medium (Reg) or serum starved in DMEM (SS) or serum starved and suspended (SS + Susp) as described in Materials and Methods, and lysates were run for Western immunoblotting. (C) Active Rac Q61L further enhances the phosphorylation at S518 for both WT and 6N merlin. Immunoblot analysis of lysates from SC4 cells that were transfected as follows: lanes, 1, vector alone; lanes 2, C6V/empty vector cotransfection; lanes 3, Cerulean-merlin-WT-Venus (C-mer WT-V)/empty vector cotransfection; lanes 4, Cerulean-merlin WT-Venus/Rac Q61L cotransfection; lanes 5, Cerulean-Merlin 6N-Venus/empty vector cotransfection; lanes 6, Cerulean-merlin 6N-Venus/Rac Q61L cotransfection; lanes 7, Cerulean-merlin 518A-Venus/empty vector cotransfection.

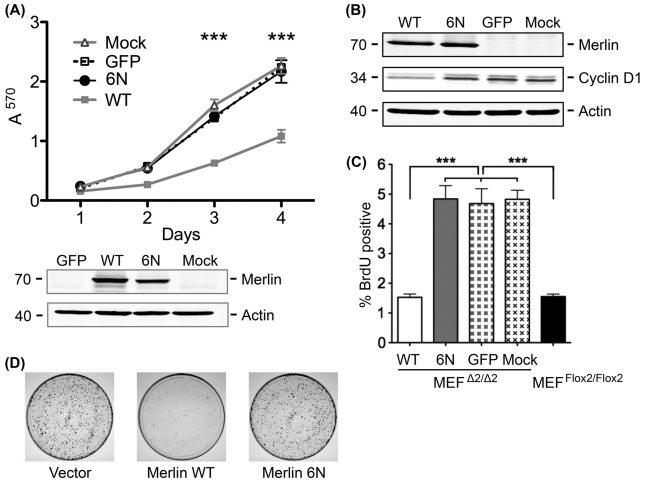

FIG. 8. FERM domain phosphoinositide binding regulates merlin's growth-suppressive function. (A) MTT assay. SC4 cells infected with merlin WT lentivirus had significantly decreased growth rate on days 3 and 4 compared to cells infected with mutant merlin 6N, GFP (control), or mock-infected cells. Error bars indicate means ± standard errors of the means. ***, $P < 0.001$ by two-way analysis of variance ($n = 3$). Expression of the recombinant merlin protein is shown in Western immunoblotting. (B) Mutant merlin 6N does not repress cyclin D1 expression. $NF2^{\Delta 2/\Delta 2}$ MEF cells were infected with the indicated adenovirus, and lysates were run for Western immunoblotting. Similar results were obtained in SC4 cells (data not shown). (C) Mutant merlin 6N does not inhibit cell proliferation. BrdU incorporation was measured as described in Materials and Methods. Reexpression of WT merlin but not mutant merlin 6N or GFP (control) in merlin-null $NF2^{\Delta 2/\Delta 2}$ MEF cells inhibits cell proliferation similar to merlin-positive $NF2^{flox2/flox2}$ MEF cells. Error bars indicate means + standard errors of the means. ***, $P < 0.001$ by one-way analysis of variance. (D) Colony formation assay. Reexpression of WT merlin but not mutant merlin 6N in SC4 cells was sufficient to significantly reduce colony formation following puromycin selection compared to vector alone. Results are representative of three independent experiments, each performed in triplicate.

less than 0.25% of all phosphoinositides is phosphorylated at the 3-position (49). PIP_2 and $PI(3,4,5)P_3$ are necessary to target proteins with polybasic clusters to the plasma membrane (23). In many cell types, approximately half of cellular PIP_2 is concentrated in cholesterol- and glycosphingolipid-rich membrane domains (39, 51). This and the flotation of merlin to the lightest fractions of a density gradient support the notion that merlin resides in such an environment.

Mutation of the PIP_2 binding sites in the ezrin FERM domain specifically abolished interaction with PIP_2 without altering ezrin folding (3). The high degree of sequence and structural similarity between the ezrin and merlin FERM domains justifies similar mutagenesis studies on merlin. Intrinsic tryptophan fluorescence and limited chymotryptic digestion of the FERM domain indicate that mutating the PIP binding site does not cause large-scale changes in the folding of the FERM domain. Circular dichroism and AUC measurements indicate that ablation of the PIP binding site does not cause large-scale changes in the secondary structure content or the size and shape of merlin. Additionally, merlin WT and 6N have similar FRET properties, providing further evidence against a large-scale conformational change induced by the 6N mutations. Functionally, the PIP_2 binding-deficient merlin efficiently binds NHE-RF, a known merlin-interacting partner, and can be phosphorylated at S518, indicating that it is accessible to the cognate kinases for this functionally important residue. Taken together, these results provide strong evidence that the FERM domain PIP_2 binding-deficient merlin folds properly.

In agreement with previous studies (31, 62), wild-type merlin is predominantly localized to regions of the plasma membrane and cell-cell boundary and colocalizes with actin. Merlin defective in FERM domain PIP binding, however, is mainly cytoplasmic and absent from the cell-cell boundary. However, we did see some cortical actin colocalization with the merlin 6N that still remains at the membrane, making it difficult for us to make a conclusive interpretation, at the level of confocal microscopy, of the need of FERM domain PIP binding in merlin colocalization with the actin cortical cytoskeleton. The partial residence of the 6N merlin mutant at the membrane may be due to the presence of the intact N-terminal 18 amino acids, an obligatory sequence for membrane attachment and for protein-protein interaction (10). FERM domain PIP binding plays a crucial role in membrane targeting of other FERM domain-containing proteins as well, including ezrin (3, 14) and PTPL1, a protein tyrosine phosphatase (4). Abolishing PIP binding greatly enhances the diffusibility of merlin, consistent with the notion that loss of PIP binding leads to detachment from the

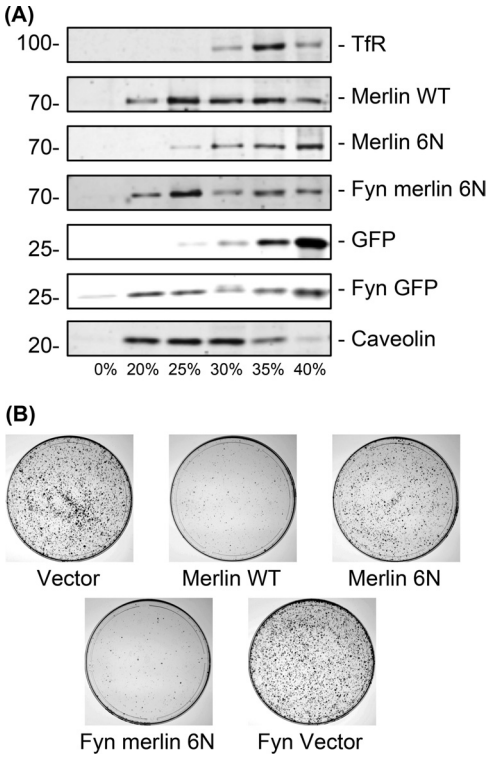

FIG. 9. Retargeting the FERM domain PIP binding-deficient mutant merlin into membrane is sufficient to restore the growth-suppressive function to the mutant merlin. (A) Fyn_{1-10} retargets the mutant merlin 6N into membrane domains. The first 10 amino acids of Fyn (Fyn_{1-10}; MGCVQCKDKE) contain a dual acylation sequence with a high affinity for membrane domains. Western immunoblots following density gradient centrifugation (OptiPrep) of transfected and confluent SC4 cell lysates shows that Fyn_{1-10} is sufficient to retarget the mutant merlin 6N into the buoyant 20% and 25% fractions, similar to proportions of wild-type merlin. Similarly, Fyn_{1-10} is sufficient to target the control GFP protein to the 20% and 25% fractions. Caveolin is mainly found in the buoyant fractions (20% and 25%), whereas transferrin receptor (TfR) is a marker for the higher-density fractions (30%, 35%, and 40%). We probed for transferrin receptor and caveolin in each case (data not shown). (B) Retargeting of the mutant merlin 6N to membrane domains using Fyn_{1-10} is sufficient to restore the colony reduction phenotype to the mutant merlin 6N. In a colony formation assay, SC4 cells transfected with merlin WT had significantly decreased number of colonies compared to cells transfected with vector alone or mutant merlin 6N following puromycin selection. However, the Fyn_{1-10} merlin 6N (which retargets the mutant merlin 6N to membrane domains) (A) is sufficient to restore the colony reduction phenotype to the mutant merlin 6N. Results are representative of two independent experiments, each performed in triplicate.

membrane or membrane-resident binding partners. Similarly, the Ras GTPase-activating protein, $GAP1^{IP4BP}$, which associates with the membrane via PIP_2, is much more mobile when rendered cytosolic (7). To our knowledge, this is the first study of merlin dynamics in mammalian cells using FRAP.

For ezrin, phosphorylation at T567 and activation require prior PIP_2 binding to the FERM domain (3, 14). For merlin, three major phosphorylation events are known: at S518 by the p21-activated kinase (29, 30, 66) and protein kinase A (PKA) (1), at T230 and S315 by Akt (63), and at S10 by PKA (34). Phosphorylation of merlin at T576, the equivalent of ezrin T567, has not yet been described in mammals, but in *Drosophila*, the Ste20 kinase, Slik, phosphorylates merlin at the equivalent residue, T616, thereby regulating its subcellular localization (25). Okada et al. (47) reported that Akt phosphorylation of merlin enhances its binding to phosphoinositides. Although FERM domain PIP binding is apparently not required for phosphorylation at S518, it is nevertheless important for the activity of merlin as a growth suppressor, as suggested by our functional data. Failure to bind PIP causes merlin to be displaced from the plasma membrane into the cytosol, and concurrently merlin loses its ability to suppress cell growth. Furthermore, restoration of membrane localization by attachment of a Fyn-based decapeptide reverses this loss of function. In view of our results, one is tempted to speculate that retargeting certain NF2 mutant proteins into membrane might restore merlin function. This cohort of mutations in NF2 patients is characterized by enhanced detergent solubility and loss of membrane association, including the point mutations K79E, Δ118 (62), and L360P (12). We are currently testing this hypothesis.

Recently, Li et al. (37) provided evidence that merlin suppresses cell growth by translocating into the nucleus, binding to the E3 ubiquitin ligase $CRL4^{DCAF1}$, and suppressing its ability to ubiquitylate target proteins. Given that this mode of merlin action is vastly different from mechanisms proposed for merlin at or near the plasma membrane (43), it is reasonable to entertain the notion that merlin is deployed in divergent, and perhaps redundant, ways to ensure that its function is fulfilled. Consistent with this notion is the fact that merlin interacts with very different subsets of proteins at the two locations (37, 43).

Finally, we do not know if FERM domain PIP binding regulates merlin protein-protein interaction, and we are currently conducting studies to test this hypothesis. It would be interesting to test if signaling pathways that impinge upon phosphoinositide homeostasis play a role in regulating merlin function; ones that do may suggest new therapeutic targets for NF2. Taken together, our data indicate that FERM domain PIP binding plays a pivotal role in membrane association, subcellular localization, and the growth-suppressive function of merlin.

ACKNOWLEDGMENTS

This work was supported by awards R01-CA78524 from the National Cancer Institute and NF043043 from the Department of Defense CDMRP Neurofibromatosis Research Program to W.I. and by funds from the Ohio Eminent Scholar program to A.B.H. T.M. was the recipient of a Young Investigator Award from the Children's Tumor Foundation. We gratefully acknowledge support from these agencies.

We are grateful to Marco Giovannini for the primary $NF2^{flox2/flox2}$ MEF cells and to Marco Giovannini and Helen Morrison for providing the SC4 cells. We thank Peixuan Guo for the use of the spectrofluorometer. We also acknowledge the support of Birgit Ehmer and Nancy Kleene at the Center for Biological Microscopy, University of Cincinnati.

REFERENCES

1. **Alfthan, K., L. Heiska, M. Gronholm, G. H. Renkema, and O. Carpen.** 2004. Cyclic AMP-dependent protein kinase phosphorylates merlin at serine 518 independently of p21-activated kinase and promotes merlin-ezrin heterodimerization. J. Biol. Chem. **279:**18559–18566.
2. **Angus, S. P., D. A. Solomon, L. Kuschel, R. F. Hennigan, and E. S. Knudsen.** 2003. Retinoblastoma tumor suppressor: analyses of dynamic behavior in living cells reveal multiple modes of regulation. Mol. Cell. Biol. **23:**8172–8188.

3. **Barret, C., C. Roy, P. Montcourrier, P. Mangeat, and V. Niggli.** 2000. Mutagenesis of the phosphatidylinositol 4,5-bisphosphate (PIP_2) binding site in the NH_2-terminal domain of ezrin correlates with its altered cellular distribution. J. Cell Biol. **151:**1067–1080.
4. **Bompard, G., M. Martin, C. Roy, F. Vignon, and G. Freiss.** 2003. Membrane targeting of protein tyrosine phosphatase PTPL1 through its FERM domain via binding to phosphatidylinositol 4,5-biphosphate. J. Cell Sci. **116:**2519–2530.
5. **Bosco, E. E., Y. Nakai, R. F. Hennigan, N. Ratner, and Y. Zheng.** 2010. NF2-deficient cells depend on the Rac1-canonical Wnt signaling pathway to promote the loss of contact inhibition of proliferation. Oncogene **29:**2540–2549.
6. **Bretscher, A., K. Edwards, and R. G. Fehon.** 2002. ERM proteins and merlin: integrators at the cell cortex. Nat. Rev. Mol. Cell Biol. **3:**586–599.
7. **Brough, D., F. Bhatti, and R. F. Irvine.** 2005. Mobility of proteins associated with the plasma membrane by interaction with inositol lipids. J. Cell Sci. **118:**3019–3025.
8. **Brown, D. A., and E. London.** 2000. Structure and function of sphingolipid- and cholesterol-rich membrane rafts. J. Biol. Chem. **275:**17221–17224.
9. **Cleveland, D. W., S. G. Fischer, M. W. Kirschner, and U. K. Laemmli.** 1977. Peptide mapping by limited proteolysis in sodium dodecyl sulfate and analysis by gel electrophoresis. J. Biol. Chem. **252:**1102–1106.
10. **Cole, B. K., M. Curto, A. W. Chan, and A. I. McClatchey.** 2008. Localization to the cortical cytoskeleton is necessary for Nf2/merlin-dependent epidermal growth factor receptor silencing. Mol. Cell. Biol. **28:**1274–1284.
11. **Curto, M., B. K. Cole, D. Lallemand, C. H. Liu, and A. I. McClatchey.** 2007. Contact-dependent inhibition of EGFR signaling by Nf2/Merlin. J. Cell Biol. **177:**893–903.
12. **Deguen, B., et al.** 1998. Impaired interaction of naturally occurring mutant NF2 protein with actin-based cytoskeleton and membrane. Hum. Mol. Genet. **7:**217–226.
13. **De Matteis, M. A., and A. Godi.** 2004. PI-loting membrane traffic. Nat. Cell Biol. **6:**487–492.
14. **Fievet, B. T., et al.** 2004. Phosphoinositide binding and phosphorylation act sequentially in the activation mechanism of ezrin. J. Cell Biol. **164:**653–659.
15. **Giovannini, M., et al.** 2000. Conditional biallelic Nf2 mutation in the mouse promotes manifestations of human neurofibromatosis type 2. Genes Dev. **14:**1617–1630.
16. **Gonzalez-Agosti, C., T. Wiederhold, M. E. Herndon, J. Gusella, and V. Ramesh.** 1999. Interdomain interaction of merlin isoforms and its influence on intermolecular binding to NHE-RF. J. Biol. Chem. **274:**34438–34442.
17. **Hamada, K., T. Shimizu, T. Matsui, S. Tsukita, and T. Hakoshima.** 2000. Structural basis of the membrane-targeting and unmasking mechanisms of the radixin FERM domain. EMBO J. **19:**4449–4462.
18. **Hanwell, D., T. Ishikawa, R. Saleki, and D. Rotin.** 2002. Trafficking and cell surface stability of the epithelial Na^+ channel expressed in epithelial Madin-Darby canine kidney cells. J. Biol. Chem. **277:**9772–9779.
19. **Hao, J. J., et al.** 2009. Phospholipase C-mediated hydrolysis of PIP2 releases ERM proteins from lymphocyte membrane. J. Cell Biol. **184:**451–462.
20. **Harder, T., P. Scheiffele, P. Verkade, and K. Simons.** 1998. Lipid domain structure of the plasma membrane revealed by patching of membrane components. J. Cell Biol. **141:**929–942.
21. **Heiska, L., et al.** 1998. Association of ezrin with intercellular adhesion molecule-1 and -2 (ICAM-1 and ICAM-2). Regulation by phosphatidylinositol 4,5-bisphosphate. J. Biol. Chem. **273:**21893–21900.
22. **Hennigan, R. F., et al.** 2010. Fluorescence resonance energy transfer analysis of merlin conformational changes. Mol. Cell. Biol. **30:**54–67.
23. **Heo, W. D., et al.** 2006. PI(3,4,5)P3 and PI(4,5)P2 lipids target proteins with polybasic clusters to the plasma membrane. Science **314:**1458–1461.
24. **Hirao, M., et al.** 1996. Regulation mechanism of ERM (ezrin/radixin/moesin) protein/plasma membrane association: possible involvement of phosphatidylinositol turnover and Rho-dependent signaling pathway. J. Cell Biol. **135:**37–51.
25. **Hughes, S. C., and R. G. Fehon.** 2006. Phosphorylation and activity of the tumor suppressor Merlin and the ERM protein Moesin are coordinately regulated by the Slik kinase. J. Cell Biol. **175:**305–313.
26. **James, M. F., et al.** 2009. NF2/merlin is a novel negative regulator of mTOR complex 1, and activation of mTORC1 is associated with meningioma and schwannoma growth. Mol. Cell. Biol. **29:**4250–4261.
27. **Johnson, W. C.** 1999. Analyzing protein circular dichroism spectra for accurate secondary structures. Proteins **35:**307–312.
28. **Kang, B. S., D. R. Cooper, Y. Devedjiev, U. Derewenda, and Z. S. Derewenda.** 2002. The structure of the FERM domain of merlin, the neurofibromatosis type 2 gene product. Acta Crystallogr. D Biol. Crystallogr. **58:**381–391.
29. **Kissil, J. L., K. C. Johnson, M. S. Eckman, and T. Jacks.** 2002. Merlin phosphorylation by p21-activated kinase 2 and effects of phosphorylation on merlin localization. J. Biol. Chem. **277:**10394–10399.
30. **Kissil, J. L., et al.** 2003. Merlin, the product of the Nf2 tumor suppressor gene, is an inhibitor of the p21-activated kinase, Pak1. Mol. Cell **12:**841–849.
31. **Lallemand, D., M. Curto, I. Saotome, M. Giovannini, and A. I. McClatchey.** 2003. NF2 deficiency promotes tumorigenesis and metastasis by destabilizing adherens junctions. Genes Dev. **17:**1090–1100.
32. **Lallemand, D., et al.** 2009. Merlin regulates transmembrane receptor accumulation and signaling at the plasma membrane in primary mouse Schwann cells and in human schwannomas. Oncogene **28:**854–865.
33. **Lallemand, D., A. L. Saint-Amaux, and M. Giovannini.** 2009. Tumor-suppression functions of merlin are independent of its role as an organizer of the actin cytoskeleton in Schwann cells. J. Cell Sci. **122:**4141–4149.
34. **Laulajainen, M., T. Muranen, O. Carpen, and M. Gronholm.** 2008. Protein kinase A-mediated phosphorylation of the NF2 tumor suppressor protein merlin at serine 10 affects the actin cytoskeleton. Oncogene **27:**3233–3243.
35. **Lepont, P., et al.** 2008. Point mutation in the NF2 gene of HEI-193 human schwannoma cells results in the expression of a merlin isoform with attenuated growth suppressive activity. Mutat. Res. **637:**142–151.
36. **Li, Q., et al.** 2007. Self-masking in an intact ERM-merlin protein: an active role for the central alpha-helical domain. J. Mol. Biol. **365:**1446–1459.
37. **Li, W., et al.** 2010. Merlin/NF2 suppresses tumorigenesis by inhibiting the E3 ubiquitin ligase CRL4(DCAF1) in the nucleus. Cell **140:**477–490.
38. **Liang, X., et al.** 2001. Heterogeneous fatty acylation of Src family kinases with polyunsaturated fatty acids regulates raft localization and signal transduction. J. Biol. Chem. **276:**30987–30994.
39. **Liu, Y., L. Casey, and L. J. Pike.** 1998. Compartmentalization of phosphatidylinositol 4,5-bisphosphate in low-density membrane domains in the absence of caveolin. Biochem. Biophys. Res. Commun. **245:**684–690.
40. **Lopez-Lago, M. A., T. Okada, M. M. Murillo, N. Socci, and F. G. Giancotti.** 2009. Loss of the tumor suppressor gene NF2, encoding merlin, constitutively activates integrin-dependent mTORC1 signaling. Mol. Cell. Biol. **29:**4235–4249.
41. **Maitra, S., R. M. Kulikauskas, H. Gavilan, and R. G. Fehon.** 2006. The tumor suppressors Merlin and Expanded function cooperatively to modulate receptor endocytosis and signaling. Curr. Biol. **16:**702–709.
42. **Matsui, T., et al.** 1998. Rho-kinase phosphorylates COOH-terminal threonines of ezrin/radixin/moesin (ERM) proteins and regulates their head-to-tail association. J. Cell Biol. **140:**647–657.
43. **McClatchey, A. I., and R. G. Fehon.** 2009. Merlin and the ERM proteins–regulators of receptor distribution and signaling at the cell cortex. Trends Cell Biol. **19:**198–206.
44. **Morrison, H., et al.** 2001. The NF2 tumor suppressor gene product, merlin, mediates contact inhibition of growth through interactions with CD44. Genes Dev. **15:**968–980.
45. **Morrison, H., et al.** 2007. Merlin/neurofibromatosis type 2 suppresses growth by inhibiting the activation of Ras and Rac. Cancer Res. **67:**520–527.
46. **Nagai, T., et al.** 2002. A variant of yellow fluorescent protein with fast and efficient maturation for cell-biological applications. Nat. Biotechnol. **20:**87–90.
47. **Okada, M., et al.** 2009. Akt phosphorylation of merlin enhances its binding to phosphatidylinositols and inhibits the tumor-suppressive activities of merlin. Cancer Res. **69:**4043–4051.
48. **Okada, T., M. Lopez-Lago, and F. G. Giancotti.** 2005. Merlin/NF-2 mediates contact inhibition of growth by suppressing recruitment of Rac to the plasma membrane. J. Cell Biol. **171:**361–371.
49. **Pendaries, C., H. Tronchere, M. Plantavid, and B. Payrastre.** 2003. Phosphoinositide signaling disorders in human diseases. FEBS Lett. **546:**25–31.
50. **Phair, R. D., and T. Misteli.** 2000. High mobility of proteins in the mammalian cell nucleus. Nature **404:**604–609.
51. **Pike, L. J., and J. M. Miller.** 1998. Cholesterol depletion delocalizes phosphatidylinositol bisphosphate and inhibits hormone-stimulated phosphatidylinositol turnover. J. Biol. Chem. **273:**22298–22304.
52. **Resh, M. D.** 2006. Palmitoylation of ligands, receptors, and intracellular signaling molecules. Sci. STKE. **2006:**re14.
53. **Rizzo, M. A., G. H. Springer, B. Granada, and D. W. Piston.** 2004. An improved cyan fluorescent protein variant useful for FRET. Nat. Biotechnol. **22:**445–449.
54. **Schuck, P.** 2000. Size-distribution analysis of macromolecules by sedimentation velocity ultracentrifugation and Lamm equation modeling. Biophys. J. **78:**1606–1619.
55. **Shaw, R. J., A. I. McClatchey, and T. Jacks.** 1998. Regulation of the neurofibromatosis type 2 tumor suppressor protein, merlin, by adhesion and growth arrest stimuli. J. Biol. Chem. **273:**7757–7764.
56. **Shaw, R. J., et al.** 2001. The Nf2 tumor suppressor, merlin, functions in Rac-dependent signaling. Dev. Cell **1:**63–72.
57. **Sherman, L., et al.** 1997. Interdomain binding mediates tumor growth suppression by the NF2 gene product. Oncogene **15:**2505–2509.
58. **Shimizu, T., et al.** 2002. Structural basis for neurofibromatosis type 2. Crystal structure of the merlin FERM domain. J. Biol. Chem. **277:**10332–10336.
59. **Shogomori, H., and D. A. Brown.** 2003. Use of detergents to study membrane rafts: the good, the bad, and the ugly. Biol. Chem. **384:**1259–1263.
60. **Sprague, B. L., and J. G. McNally.** 2005. FRAP analysis of binding: proper and fitting. Trends Cell Biol. **15:**84–91.
61. **Stickney, J. T., W. C. Bacon, M. Rojas, N. Ratner, and W. Ip.** 2004. Activation of the tumor suppressor merlin modulates its interaction with lipid rafts. Cancer Res. **64:**2717–2724.

62. **Stokowski, R. P., and D. R. Cox.** 2000. Functional analysis of the neurofibromatosis type 2 protein by means of disease-causing point mutations. Am. J. Hum. Genet. **66:**873–891.
63. **Tang, X., et al.** 2007. Akt phosphorylation regulates the tumour-suppressor merlin through ubiquitination and degradation. Nat. Cell Biol. **9:**1199–1207.
64. **Thankamony, S. P., and W. Knudson.** 2006. Acylation of CD44 and its association with lipid rafts are required for receptor and hyaluronan endocytosis. J. Biol. Chem. **281:**34601–34609.
65. **Whitmore, L., and B. A. Wallace.** 2004. DICHROWEB, an online server for protein secondary structure analyses from circular dichroism spectroscopic data. Nucleic Acids Res. **32:**W668–W673.
66. **Xiao, G. H., A. Beeser, J. Chernoff, and J. R. Testa.** 2002. p21-activated kinase links Rac/Cdc42 signaling to merlin. J. Biol. Chem. **277:**883–886.
67. **Xiao, G. H., et al.** 2005. The NF2 tumor suppressor gene product, merlin, inhibits cell proliferation and cell cycle progression by repressing cyclin D1 expression. Mol. Cell. Biol. **25:**2384–2394.
68. **Zacharias, D. A., J. D. Violin, A. C. Newton, and R. Y. Tsien.** 2002. Partitioning of lipid-modified monomeric GFPs into membrane microdomains of live cells. Science **296:**913–916.